1. Introduction

1A. CBD vs. CNS: Computational NeuroScience models neurons and neural networks well, brains poorly. The limitation of CNS stems from its failure to deal with the hierarchical organization of brains. At the cellular level the key module is the neuron. Network theory works well modeling sensorimotor systems to and from cortex in vertebrate brain stem and spinal cord and in ganglionic chains of invertebrate 'simpler systems'. At the brain level the key module for Computational Brain Dynamics is cortex. Each neuron interacts with many thousand other neurons in tissue — laminated neuropil. Neuropil can't be reduced to networks of equivalent neurons; it has differing architectures, state variables, and operations by which it creates and processes information. **CBD** and **CNS** require differing definitions, premises, rules of evidence, and classic experiments, recalling the differences between thermodynamics and statistical mechanics.

In **CNS** experiments a brief stimulus is typically confined to a single sense modality. The resulting unit activity is tracked through relays that process the stimulus information, and a network is constructed to simulate the processing. In **CBD** experiments the subjects deal not with isolated stimuli but with environmental situations, which are signaled by swarms of sensory receptor action potentials that propagate into spinal cord and brain, where they modify pre-existing unit activity. The impact of a unit swarm destabilizes cortical neuropil, causing it to jump itinerantly through successive states. **CBD** models these states and state transitions as large-scale spatial patterns of neural activity that rather quickly lead to motor activity governing the multisensory engagement of animals with their situations. The cortical states resemble frames in a motion picture. The rules of evidence in **CBD** require that brain states be defined as spatial patterns formed by state transitions; that state variables include carrier waveforms and gating frequencies; and that EEG parameters be validated as meaningful by demonstrating correlations among EEG patterns, environmental situations, subjects' behaviors, and human subjects' descriptions of multi-sensory perceptions (Gestalts) and their meanings [Freeman, 2003].

1B. EEG: Dendritic current regulates action potentials. That same current in cortex is the main source of the electroencephalogram (EEG) as it flows across the fixed extracellular impedance of the neuropil. Due to summation of extracellular electric potentials of dendrites that are oriented in palisades in cortical neuropil, the EEG amplitude expresses the local mean field of unit activity in the neighborhoods of interacting pyramidal cells. This feature endows the EEG with its value for estimating the magnitudes of spatial state variables in neuropil at the brain level.

Scalp EEG has value for both **CNS** and **CBD** in cognitive studies, because it accesses a large spatial area of neuropil at high temporal resolution and much higher spatial resolution than has been appreciated. **CNS** sees cortex as a network of modules. It regards the EEG as a mixture of time-dependent signals like voices at a cocktail party, so it localizes the signals with high-pass spatial filters (Laplacian operators for EEG, synthetic aperture magnetometry for MEG) to focus modular signals, and uses PCA/ICA to represent them by equivalent dipoles. **CBD** sees cortical signals as nonlocal due to widespread interactions in neuropil. The coordinated activity is observed in EEG through low-pass spatial filters. Spatial patterns are described by high-dimensional vectors with tips having itinerant chaotic trajectories [Tsuda, 1961] in brain state space. Sequential AM patterns vary in size, outline and textures that correlate with

cognitive situational behaviors of the kind documented by Köhler's Gestalt theory [1940], Tolman's cognitive map [1948], and Gibson's ecological psychology [1979].

1C. Neocortex: CNS treats inadequately the evolution of cortex [Herrick, 1948]. The first laminated neuropil in primordial vertebrates such as the salamander, 3-layered archicortex (hippocampus) and paleocortex (the olfactory system), formed a unified sheet comprising each cerebral hemisphere. The best 'simpler system' for modeling elementary brain dynamics is olfaction, not vision or audition; the best animal models are rats and rabbits, not monkeys or humans. Paleocortex in mammals is supplemented with a far more complex form of neuropil: 6-layered neocortex. Despite its enormous size in humans, neocortex retains its anatomical unity and its dynamics for extremely rapid, repetitive state transition and spatial pattern formation. The specialized **CNS** neural networks embedded in neocortex operate as input/output interfaces for seeing, hearing, touching and intentional action. Understanding their roles in perception will require new methods of EEG analysis that are given by a new **CBD** model.

1D. K-sets: The new model is an extension of a hierarchy of nonlinear ordinary differential equations with noninteractive populations (KO) near equilibrium at its base [Freeman, 1975; Principe et al., 2001]. By synaptic transmission KO sets create interactive populations of excitatory (KIe) or inhibitory (KIi) neurons with nonequilibrium point attractors. KI populations of olfactory excitatory or inhibitory neurons comprise the KII set having also a limit cycle attractor used to model olfactory bulb or prepyriform cortex. The KIII set incorporates 3 KII sets to model chaotic attractors governing the olfactory EEG [Freeman, 1987], and to replicate olfactory capacity for classification of incomplete patterns embedded in complex backgrounds with facilitation by noise [Freeman et al., 1997; Kozma & Freeman, 2001]. The KIV model of the primordial amphibian paleocortex comprising its limbic system is currently under development as an interactive network of 3 KIII sets being used by autonomous vehicles for navigation [Kozma, Freeman & Erdí, 2003]. The new goal is to construct a KV set that models the unique neurodynamics of neocortex found only in mammals.

Anatomical data already make clear that neocortical neuropil cannot be modeled as a random graph with uniform probability of connection lengths. Short connections approximating nearest neighbor predominate, but the significant proportion of long connections leads to small-world effects [Watts & Strogatz, 1998]. Several types of network have been proposed to model the long-distance synchronization that is readily observed in scalp EEG [Rodriguez et al., 1999; Friston, 2000; Linkenkaer-Hansen et al., 2001; Varela et al., 2001; Stam et al., 2003]. Quantitative anatomical data have for years [Sholl, 1956] shown exponential connectivity distributions among cortical neurons; more recent data [Braitenberg & Schüz, 1991] show fractal and power-law distributions of cortical connectivity that characterize scale-free networks [Wang & Chen, 2003]. The goal in **CBD** goal is to model neocortex as stabilized in a state of self-organized criticality [Bak, 1996; Jensen, 1998].

2. Spatial patterns of gamma in paleocortical (OB) and neocortical EEG

2A. Paleocortex: Initial construction of K-sets was by measurement and simulation of impulse responses (evoked potentials and poststimulus time histograms) of olfactory neurons to electrical stimuli [Freeman, 1975]. The K-sets were extended to measurement and

simulation of changes in background EEG and unit activity in the olfactory system in response to odorant conditioned stimuli with reinforcement (CS+) and without reinforcement (CS-) after discriminative training [Freeman & Grajski, 1987]; CS information was encoded in spatial patterns of amplitude modulation (AM) of spatially coherent gamma oscillations (Fig. 01, A) that were accompanied by spatial patterns of phase modulation (PM) (Fig. 02, B). The method used high-density 8x8 arrays of implanted electrodes to resolve EEG spatial texture. The demonstration was generalized to the visual, auditory and somatic cortices with multichannel EEGs from trained rabbits [Barrie, Freeman & Lenhart, 1996] and gerbils [Ohl, Scheich & Freeman, 2001].

EEG measurement requires elementary waves and geometric shapes called "basis functions" [Freeman, 1975]. Basis functions are adjusted and added like weights on a scale until their sum matches the wave pattern to "decompose" into its numbered parts. The basis functions tested for temporal patterns came from FFT, PCA, ICA, ARMA, Gabor filters, or nonlinear wavelets [Freeman & Viana Di Prisco, 1986]. None of these was fully appropriate for long segments (>256 ms) with broad 1/f-type spectra. The most effective basis functions in brief epochs (32-256 ms) were rms for amplitude and a cosine for phase, owing to slow frequency modulation about the mean within short epochs.

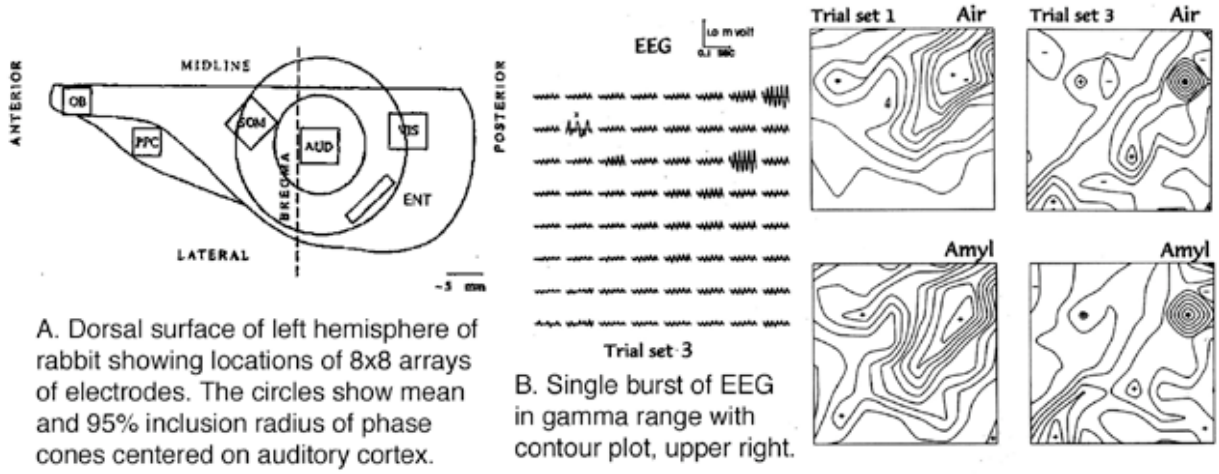

A. Dorsal surface of left hemisphere of rabbit showing locations of 8x8 arrays of electrodes. The circles show mean and 95% inclusion radius of phase cones centered on auditory cortex.

B. Single burst of EEG in gamma range with contour plot, upper right.

Fig. 01. A. Squares show the locations of intracranial high-density 8x8 electrode arrays over the primary sensory areas of the left hemisphere of the rabbit brain. Circles show median and 95% diameter of spatial patterns of phase (half-power phase cone diameters centered on the auditory array). From Barrie, Freeman & Lenhart [1996]. **B.** The AM patterns (spatial amplitude modulation of the gamma carrier wave) are shown as contour plots of the root mean square (rms) amplitude of bulbar EEG before and during an odor stimulus. The patterns change with the situation in classical conditioning. From Freeman [2000].

The optimal basis function for spatial patterns of amplitude was the bivariate Gaussian [Freeman & Baird, 1987]. For spatial patterns of phase in the olfactory bulb, a plane fit the phase gradient of the impulse response (averaged evoked potential) on electrical stimulation of the olfactory nerve, giving a phase velocity equal to the conduction velocity of the afferent axons. The phase gradient of the bursts of gamma EEG induced by inhalation was not a plane. The conic basis function best minimized by far the least squares residuals of surface-fitting [Freeman and Baird, 1987]. The location and sign of the

apex (phase lead or lag) varied randomly over successive inhalations. **Phase cones were abolished in controls by randomization of channel order, by shuffling (transposition of segments), or by calculating surrogate data** [Freeman, in press]. In OB each inhalation gave a spatial pattern of amplitude modulation (AM) of the shared bulbar gamma wave (Fig. 01, B) that could be used to classify EEG segments with respect to learned odorant stimuli (Fig. 02, A) [Freeman and Grajski, 1987]. Each AM pattern also had phase modulation (PM, Fig. 02, B) - the phase cone - , which was interpreted as the residue of a state transition that was induced by inhalation. Neuropil being a distributed medium, a state transition spread from a site of nucleation (apex); the phase gradient was set by the conduction velocity of the axons parallel to the surface and by the frequency of the induced oscillation.

2B. Neocortex: The neocortical EEGs of the visual, auditory and somatic cortices showed that, following classical and operant conditioning of animals to discriminate conditioned stimuli in these modalities, a sequence of 2-4 AM patterns occurred in the gamma carrier wave. The intermittent AM patterns were classified at better than chance levels ($p<.01$) with respect to the conditioned stimuli on randomly alternating trials [Barrie, Freeman & Lenhart, 1996; Ohl, Scheich & Freeman, 2001]. The hypothesis was confirmed that each AM pattern was formed by an input-dependent state transition that was manifested in a phase cone [Freeman, 2003] broad enough to include multiple sub-areas of sensory cortices (circles, Fig. 01, A).

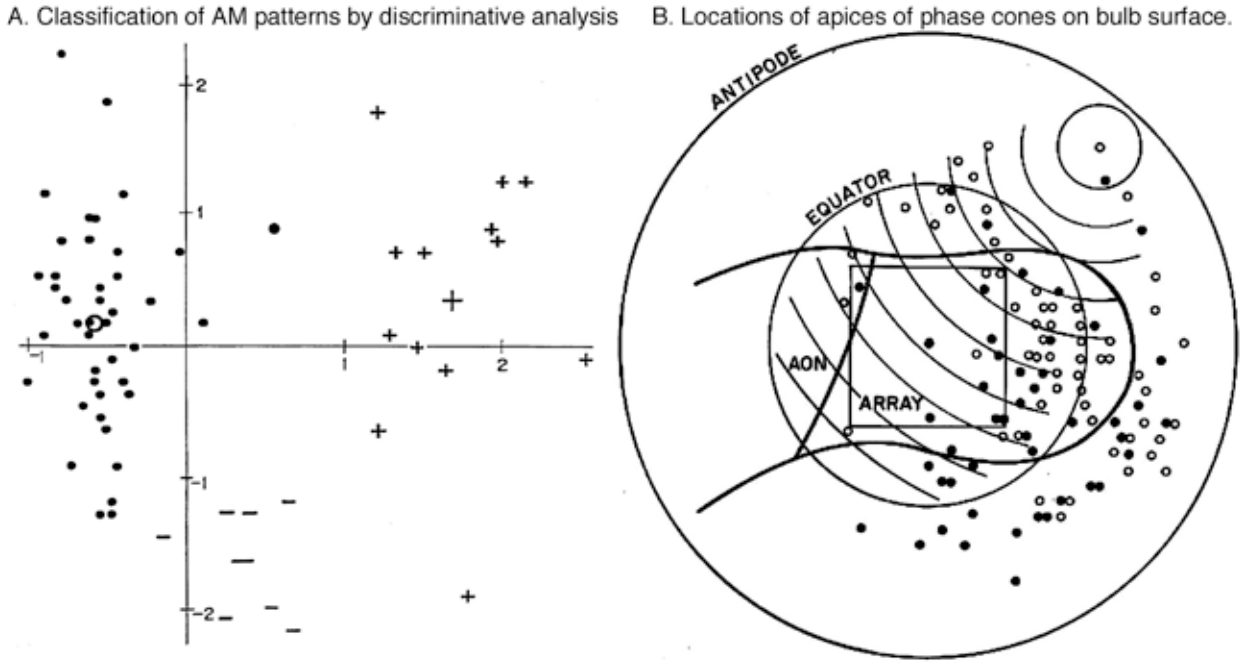

Fig. 02. A. AM patterns of EEG gamma bursts had >95% of variance in the 1st component of PCA. The RMS of each AM pattern gave a point in 64-space. Similar patterns formed clusters, shown here by stepwise discriminant analysis. The clusters show chaotic attractors in brain state space, projected into 2-space. From Freeman & Viana Di Prisco [1986]. **B.** The square shows the outline of the 8x8 array [5.6 x 5.6 mm] on the surface of rabbit OB (dark outline). The spherical bulbar surface was flattened to plot the locations of the apices of phase cones from 40 trials. The spatial pattern of phase modulation (PM)

conformed to a cone as shown for one burst with isophase contours at intervals of 0.1 rad. The location and sign of the apices varied randomly as shown by filled dots (phase lead) and open dots (phase lag). This PM pattern in the OB was found in all neocortical sensory areas [Freeman & Barrie, 2000; Freeman, 2003]. From Freeman & Baird [1987]

In all areas the classificatory information in the AM patterns was nonlocal; no one electrode was more or less important than any other; the more channels the better the classification [Freeman & Baird, 1987; Barrie, Freeman & Lenhart, 1996; Kozma & Freeman, 2002; Ohl et al., 2003]. This nonlocality of EEG classificatory information is a characteristic of perception that distinguishes it from sensory information that is localized by unit recording.

2C. Hemisphere-wide spatial EEG patterns: Further generalization was achieved by recording EEGs simultaneously from mini-arrays on the left visual, auditory, somatic, olfactory and entorhinal areas of cats and rabbits trained to discriminate CS+/-. The phase and amplitude of the 64 EEG signals were calculated in the species-specific gamma range for each subject [Freeman, Gáal & Jornten, 2003]. Two to three recursive spatial AM patterns were detected between CS and CR that served to classify EEG segments with respect to CS+ and CS- (Fig. 03, A). The classificatory information was in all recording sites. Removal of data from any of the 5 areas reduced correct classification, proving that the memory was distributed and dynamic, not local and static. The largest reduction in goodness of classification resulted from removing the data from the olfactory bulb channels [Freeman & Burke, 2003].

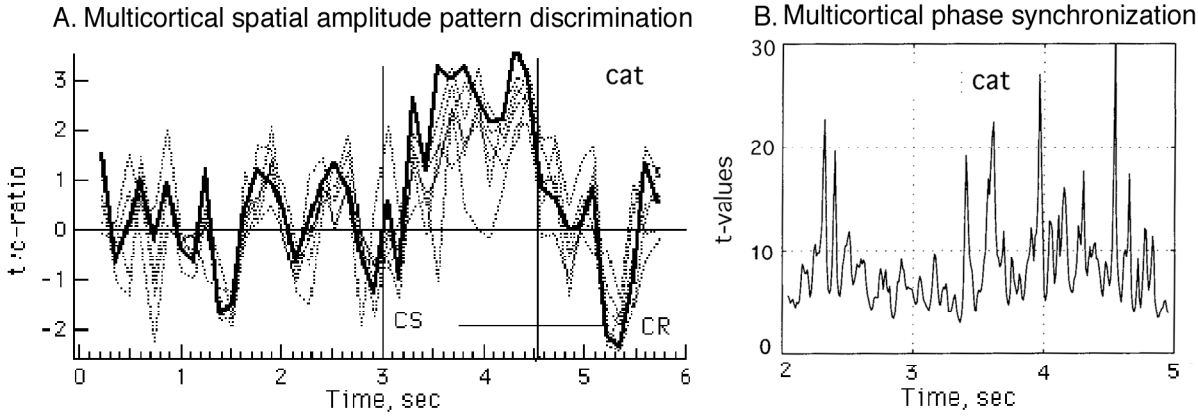

Fig. 03. Neocortical EEG lacked the burst structure of paleocortical EEG that served to locate state transitions dependent on input. Classification of the rms AM patterns across 40 trials was done in a moving window 64-128 msec in duration, stepped at 8 msec overlapping intervals. At each step the number of correctly classified patterns among the 40 AM patterns (20 CS+ and 20 CS- randomly interspersed) was calculated. In previous studies of neocortex [Barrie, Freeman & Lenhart, 1996] the 64 electrodes were concentrated on one sensory cortex. Here there were 5 mini-arrays on the left hemisphere. **A.** The dark curve shows the level of pattern classification of global EEG segments from randomly interspersed trials in cats with reinforced and unreinforced conditioned stimuli. The dotted curves show the decrease in significance level when the data were excluded from the visual, auditory, somatic, olfactory, or entorhinal areas, showing that all areas contributed to the classification. From Freeman & Burke [2003]. **B.** The curve shows synchronization among the 5 areas, measured by the analytic phase. From Freeman & Rogers [2003].

The analytic phase from the Hilbert Transform gave a synchronization index [Tass et al., 1998] that revealed intermittent phase locking of the gamma EEG among all five areas, correlated with maxima in AM pattern classification (Fig. 03, B) [Freeman & Rogers, 2002, 2003]. These data led to the hypothesis that global spatial patterns formed by repetitive state transitions over much if not all of each cerebral hemisphere, large enough to integrate the several primary sensory areas in the formation of multisensory percepts (Gestalts).

3. Human intracranial and scalp EEG from high-density arrays

3A. Spatial PSDx to set Nyquist frequencies: The basic requirement for spatial pattern analysis is spatial spectral analysis by over-sampling the EEG with a linear array to calculate the spatial power spectral density (PSDx). The concave-upward inflection (Fig. 04, A) defines the upper frequency limit at which noise predominates. That spatial frequency determines the Nyquist frequency, and the spatial electrode interval is half that spatial wavelength. Then an electrode array with that interval will not miss spatial texture nor will the spectra suffer aliasing. This work was done 30 years ago to study EEG patterns in animals. Four years ago for intracranial studies in humans a 1x64 linear array was designed with spacing of 0.5 mm and length 32 mm, short enough to fit onto a single gyrus in neurosurgical patients during exploration to treat epilepsy [Freeman et al., 2000]. The PSDx (Fig. 04, A, right curve) indicated an optimal sample interval of 1.25 mm, an order of magnitude closer than the standard clinical array interval of 1 cm to search for textural patterns in subdural EEG. The PSDx showed the $1/f^{\alpha}$ form in log-log coordinates already found in animals with $\alpha \sim 2 \pm 1$.

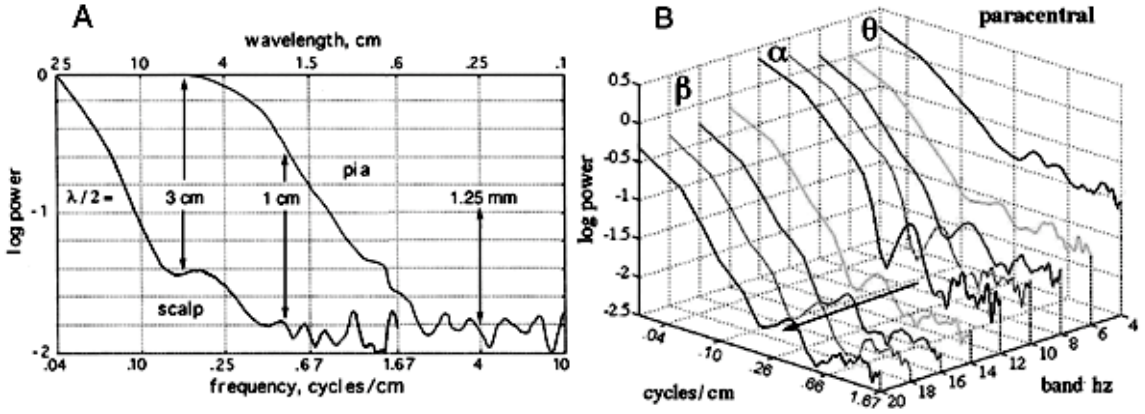

Fig. 04. A, pia: Spatial power spectral density (PSDx) from a linear array on a single gyrus in a human subject with spacing of 0.5 mm [Freeman et al., 2000] showing '1/f' scaling. **'Scalp':** PSDx from curvilinear scalp array with spacing of 3 mm revealed a peak in the spatial frequency range of gyri and sulci. From Freeman et al. [2000]. **B.** The PSDx of scalp EEG in narrow temporal bands gave the peak in all temporal bands through the gamma range (not included here). That spread was the PSDt pattern of a temporal impulse that occurred synchronously over 10-19 cm distance on the scalp and repeated nearly periodically in the alpha-theta range. The spatial resolution of gamma activity in scalp EEG extended to frequencies approaching the width of gyri. From Freeman et al. [2003].

A linear 1x64 array was designed for scalp EEG with spacing of 3 mm and length 18.9 cm. The PSDx (Fig. 04, A, left curve) was not $1/f^{\alpha}$ in form, partly owing to more rapid fall in log power with increasing log frequency imposed by the impedance of the skull and scalp, and partly due to a spatial spectral peak in the middle spatial frequency range that corresponded to the spatial frequency of the gyri and sulci of the human cerebral hemisphere [Freeman et al., 2003]. Derivation of the PSDx in each band of temporally band pass filtered EEG showed that this spatial peak occurred in all temporal frequency bands through beta (Fig. 04, B) and gamma (not reproduced here). This peak in PSDx implied that a temporal EEG impulse was repeatedly synchronized over distances of 10 to 19 cm covering multiple gyri and sulci.

3B. Aperiodic phase re-setting of beta-gamma oscillations at alpha-theta rates: This inference gave the hypothesis that the high temporal resolution of instantaneous frequency and phase afforded by Hilbert Transform (HT) would enable detection of the simultaneous jumps in phase over wide areas of the scalp EEG that would demarcate state transitions by which neocortex repeatedly re-synchronized beta and gamma oscillations in broad spatial domains. This hypothesis was tested and verified [Fig. 05, Freeman, Burke & Holmes, 2003] in normal human volunteers at rest with eyes closed giving prominent alpha activity, and with eyes open and fixated or engaged in generating weak but controlled electromyographic activity (EMG) by tensing scalp muscles, both of which were intentional actions without overt bodily movements.

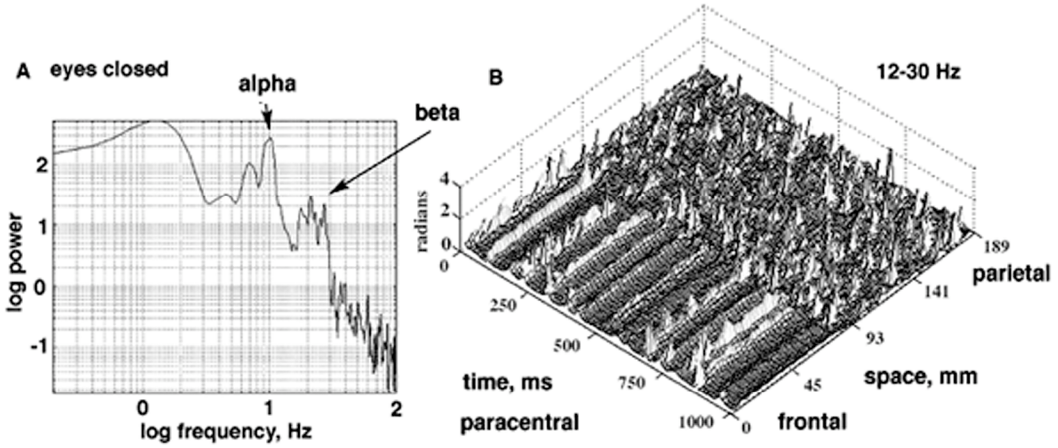

Fig. 05. A. The cospectrum of the crosscorrelation between the unfiltered EEG and the analytic phase differences on every channel shows peaks in the alpha and beta ranges. **B.** The coordinated analytic phase differences (CAPD) calculated for the 64 channels after band pass filtering in the beta range (12-30 Hz) revealed episodic plateaus of phase constancy that were bracketed by jumps in phase that were synchronized over distances varying from a few cm to the entire linear array. The spatial standard deviation, $SD_x(t)$, of the CAPD gave a reliable measure of spatial synchrony in scalp EEG. AM patterns are to be sought in plateaus bracketed by phase slip. From Freeman, Burke & Holmes [2003].

Band-pass filtering enabled application to the broad-spectrum EEG [Freeman, Burke & Holmes, 2003]. To find the optimum pass band the rate of change in analytic frequency, ω, was calculated from successive phase differences. These revealed plateaus of phase

constancy bracketed by changes in CAPD that took place simultaneously over extended portions (Fig. 05, B) and at times the entire array. The jumps in w recurred at rates in the alpha-theta ranges (Fig. 05, A). The pass band for the HT was optimized by cross-correlating □ with the unfiltered EEG repeatedly while varying the cut-off frequencies and measuring the cospectral peak in the alpha range to construct tuning curves for 9 subjects; all gave optimal filters in the beta band, 12-30 Hz.

Application of the HT to multiple EEG from an N-array was complicated by the fact that the N phase values in a stable epoch are distributed in a conic pattern, so that analytic phase from the arctangent gives phase vectors from each electrode that rotate across the imaginary axis at different times. When phase values were unwrapped, the parallel ramps diverged unpredictably in offsets of □ or 2□. This problem is solved either by calculating sequential phase differences for the CAPD (instantaneous frequency, Fig. 05, B), or by restricting measurement of phase cones to time intervals between first and last crossings of the imaginary axis by the vectors (Table 1).

3C. Comparison of phase from Fourier and Hilbert transforms: Two basic quantities were essential to describe spatial patterns of phase: the mean temporal wavelength, W_T, in rad/sec and the mean spatial wavelength, W_X in rad/mm [Freeman, in press]. Table 1 compares summary values of W_T and W_L from the Fourier and Hilbert methods. A statistically significant difference was found only for the phase gradient. This difference was traced to the procedural difference that the FFT was restricted to epochs ≥32 msec in order to measure frequency in the gamma range from which to calculate the phase, whereas the HT was restricted to epochs ≤12 msec in order to avoid the breaks imposed by the calculation of the arctangent.

Table 1. Mean ± SD of phase parameters: FFT/Hilbert

subject	N/s	frequency	gradient	W_T	W_X
N = 6 rabbits		Hz	rad/mm	ms/rad	mm/rad
Mean FFT	10.2	32.7±4.8	.111±.040[b]	5.36±1.38	11.4±4.1
Mean HT	32.4	38.8±4.3	.158±.048[b]	4.41±0.46	7.7±2.7
N = 1					
Human FFT[a]	5.1	26.5±1.9	.066±.017[c]	6.0±0.4	15.5±4.7
Human HT[a]	21.7	31.5±3.8	.092±.030[c]	5.13±0.70	11.7±3.9

[a] From Freeman (in press), 25-50 Hz, window 200 ms, <30% residuals. [b] $p < .01$. [c] $p < .001$.

Table 1. The two basic parameters of neocortical EEG, temporal wavelength, W_t, and spatial wavelength, W_x, were evaluated by the FFT and HT methods. The steeper gradient by HT was due to its short window. Convergence of the spatial parameters by FFT/HT proved success in solving the HT problem of multiple channels. From Freeman, [in press].

Table 1 illustrates the types of measurement that are required in order to validate the measures with HT by correlation with those by FFT, and to compare the spatiotemporal properties of phase in humans with those in animals. Data are listed for W_L and W_X from a 1x1 cm 8x8 grid in a human subject. The means and SD of phase gradients were lower for humans than for animals. However, analysis showed [Freeman, in press] that the parameters of phase cones and the derived measures of cone diameter and duration were **fractal** [Linkenkaer-Hansen et al., 1999], and that the means and SD varied with the duration

of temporal windows and the size of electrode arrays. The human grid was 50% larger than the rabbit grid, and so were the phase parameters, which implied that the local dynamics in rabbit and human neocortex are basically the same, though human brains are larger.

4. Modeling neocortical dynamics with the KV set

These data, combined with those illustrated in Fig. 02, reveal a fundamental difference between the 3-layered paleocortex (as embodied in the olfactory bulb) and 6-layered neocortex. In the OB only one phase cone at a time covers the bulb with each inhalation, as shown by a single apex with multiple phase gradients for different frequencies but invariant phase velocity. In neocortices multiple phase cones overlap at all times, each with its own apex and gradient. Under the interpretation that phase cones represent local state transitions, they resemble bubbles in a pan of boiling water. **This difference between 3-layered paleocortex and 6-layered neocortex has great theoretical significance, because it indicates that, unlike the OB, neocortex is stabilized in a state of self-organized criticality [Bak, 1996; Jensen, 1998].** The classic model for SOC is the sand pile that maintains its critical slope by repeated avalanches having random locations and fractal distributions of size and duration. The implication is that neocortex maintains a stable state through local feedback control of neural firing rates everywhere in neocortex [Freeman, 1975, 2000] by homeostatically regulating the gain of synaptic interaction. The mean level of firing rates is comparable to the critical angle of the sand pile, and to the transition temperature of a pan of boiling water. The generalized feedback gain constitutes an order parameter [Haken, 1983]. In this context the peaks in the power spectrum show oscillations that are equivalent to avalanches by which neocortex maintains its stability under perturbation by sensory and other control parameters, mainly thalamic [Miller & Scheiner, 2000]. The fractal distributions imply that the state of SOC is scale-free [Wang and Chen, 2003]. CAPD are invariably found in EEG from intracranial grids fixed in rabbits and the human subject. There are no normative sizes, durations or numbers of neocortical phase cones or CAPD; the CAPD jumps in scalp EEG may constitute the tails of fractal distributions, which represent neocortical state transitions that extend widely over each hemisphere and may include multiple sensory areas in the formation of Gestalts.

Documenting the spatiotemporal phase infrastructure of neocortical EEG is critical for guiding the design of small-world, scale-free networks to model the dynamics by which neocortex combines flexibility with stability and integrates multisensory information with memory into Gestalts. For example, a key finding to be explained is the random variation in phase cones between maximal lead (“explosion”) and maximal lag (“implosion”) at the apex (Fig.02, B), which might be modeled as a saddle node or subcritical Hopf bifurcation in a scale-free network.

5. References: citations to sources of Figures 1-5 and Table 1.

Bak P [1996] How Nature Works: The Science of Self-organized Criticality. New York: Copernicus.

Barrie JM, Freeman WJ, Lenhart M [1996] Modulation by discriminative training of spatial patterns of gamma EEG amplitude and phase in neocortex of rabbits. J Neurophysiol 76: 520-539.

Braitenberg V, Schüz A [1991] Anatomy of the Cortex: Statistics and Geometry. Berlin: Springer-Verlag.

Freeman WJ [1975] Mass Action in the Nervous System. New York: Academic Press. Available in electronic form at http://sulcus.berkeley.edu

Freeman WJ [2000] Neurodynamics: An Exploration of Mesoscopic Brain Dynamics. London UK: Springer-Verlag.

Freeman WJ [2003] A neurobiological theory of meaning in perception. Part 2. Spatial patterns of phase in gamma EEG from primary sensory cortices reveal the properties of mesoscopic wave packets. Int J Bifurc Chaos 13: 2513-2535.

Freeman WJ [in press] Origin, structure, and role of background EEG activity. Part 2. Analytic phase. Clin. Neurophysiol.

Freeman WJ, Barrie JM [2000] Analysis of spatial patterns of phase in neocortical gamma EEGs in rabbit. Journal of Neurophysiology 84: 1266-1278.

Freeman WJ, Burke BC [2003] A neurobiological theory of meaning in perception. Part 4. Multicortical patterns of amplitude modulation in gamma EEG. Int J Bifurc Chaos 13: 2857-2866

Freeman WJ, Burke BC, Holmes MD [2003] Aperiodic phase re-setting in scalp EEG of beta-gamma oscillations by state transitions at alpha-theta rates. Hum Brain Mapp 19:248-272.

Freeman WJ, Burke BC, Holmes, MD, Vanhatalo S [2003] Spatial spectra of scalp EEG and EMG from awake humans. Clin Neurophysiol 114: 1055-1060.

Freeman WJ, Rogers LJ [2003] A neurobiological theory of meaning in perception. Part 5. Multicortical patterns of phase modulation in gamma EEG. Int J Bifurc Chaos 13: 2867-2887.

Freeman WJ, Rogers LJ, Holmes MD, Silbergeld DL [2000] Spatial spectral analysis of human electrocorticograms including the alpha and gamma bands. J Neuro Meth 95: 111-121.

Jensen HJ [1998] Self-Organized Criticality: Emergent Complex Behavior in Physical and Biological Systems. New York: Cambridge.

Kozma R, Freeman WJ, Erdí P [2003] The KIV model – nonlinear spatio-temporal dynamics of the primordial vertebrate forebrain. Neurocomputing 52: 819-826.

Linkenkaer-Hansen K, Nikouline VM, Palva, JM, Iimoniemi RJ [2001] Long-range temporal correlations and scaling behavior in human brain oscillations. J Neurosci 15: 1370-1377.

Ohl FW, Scheich H, Freeman WJ [2001] Change in pattern of ongoing cortical activity with auditory category learning. Nature 412: 733-736.

Principe JC, Tavares VG, Harris JG, Freeman W.J [2001] Design and implementation of a biologically realistic olfactory cortex in analog VLSI. Proc IEEE 89: 1030-1051.

Stam CJ, Breakspear M, van Cappellen van Walsum A-M, van Dijk BW [2003] Nonlinear synchronization in EEG and whole-head recordings of healthy subjects. Hum Brain Mapp 19:63-78.

Varela F, Lachaux J-P, Rodriguez E, Martinerie J [2001] The brain-web: phase synchronization and large-scale integration. Nature Rev Neurosci 2:229-239.

Wang XF, Chen GR [2003] Complex networks: small-world, scale-free and beyond. IEEE Circuits Syst 31: 6-20.

Watts DJ, Strogatz SH [1998] Collective dynamics of 'small-world' networks. Nature 393: 440-442.

Other references cited in this review are published in the above research reports.

This study was supported by grant MH 06686 from the National Institute of Mental Health, grant NCC 2-1244 from the National Aeronautics and Space Administration, and grant EIA-0130352 from the National Science Foundation to Robert Kozma.